Adsorption of Cs on Si(111)7×7: Studies of photoemission from surface states and core levels

K. O. Magnusson,* S. Wiklund, R. Dudde,† and B. Reihl‡
Department of Synchrotron Radiation Physics, University of Lund, Sölvegatan 14, S-223 62 Lund, Sweden
(Received 11 March 1991)

We have studied the development of the electronic structure at the early stages of interface formation of Cs on the Si(111)7×7 surface. Low-energy electron diffraction shows that the 7×7 surface symmetry is conserved throughout the sub-saturation-coverage region. The changes in the surface electronic states characteristic of the clean silicon surface and the development of Cs-induced surface electronic states with increasing Cs coverage have been studied with angle-resolved ultraviolet photoelectron spectroscopy. Changes observed predominantly in the emission from the adatom dangling-bond state suggest that bonding of Cs occurs primarily at the adatom site on the Si(111)7×7 surface. At two-thirds of the saturation coverage, a strong Cs-induced surface state dominates the valence-band region. This state exhibits a downward dispersion along the high-symmetry lines in going away from normal emission, thus proving the semiconducting state of this well-ordered Si(111)7×7-Cs surface. Continued adsorption takes place at the rest-atom sites, making the surface metallic as the coverage reaches saturation. The metallicity is evident from the Fermi cutoff in valence-band photoemission and from the asymmetric broadening of the Cs 4*d* states, characteristic of metallic materials. Studies of the Si 2*p* level reveal changes in the line shape, which can be modeled with changes in surface core-level shifts and introduction of asymmetric broadening. These observations suggest that metallization occurs through the development of states at the Fermi level of both Cs and Si character. Studies of the Si 2*p* level further show an upward band bending with a maximum of 0.38 eV at the saturation coverage.

I. INTRODUCTION

The electronic structure of the Si(111)7×7 surface is probably the most studied semiconductor surface. Photoemission techniques have shown the appearance of three filled surface states, the topmost situated at the Fermi level (E_F) rendering the surface metallic.[1–3] Inverse photoemission has revealed an empty surface state[4,5] and studies using scanning-tunneling microscopy (STM) in spectroscopic mode have identified the origin of these states.[6] The STM results have also strongly supported the dimer–adatom–stacking-fault (DAS) model[7] for the geometry of the Si(111)7×7 surface.

This silicon surface, obtained by annealing, has frequently been used as a model substrate in studies of metal adsorption on semiconductor surfaces. Recently the problem of alkali-metal adsorption has been applied to the Si(111)7×7 surface[8] where the influence of Cs and K on the surface electronic structure was studied as a function of coverage. With the use of angle-integrated ultraviolet photoelectron spectroscopy (UPS) and angle-resolved inverse photoemission it was shown that adsorption takes place at the adatoms on the surface, affecting preferentially the surface states originating from dangling-bond orbitals on these atoms. In both cases the surfaces were found to be semiconducting at saturation of the work function, while it was stated that continued exposure of Cs changed the state of that surface back to metallic again.[8]

In this paper we present the results of angle-resolved UPS (ARUPS) studies of the photoemission from surface states and core levels during the adsorption of Cs on the Si(111)7×7 surface. The results show that the Cs-induced topmost filled surface state is most intense at two-thirds of the saturation coverage and the dispersion of this state reveals the semiconducting state of the Si(111)7×7-Cs surface. The metallization of the surface by continued exposure to Cs beyond the saturation coverage is confirmed through the observation of a Fermi cutoff developing in the valence-band photoemission and of asymmetric broadening of the Cs 4*d* core level, characteristic of metallic behavior. The latter shows that metallization occurs in the alkali-metal overlayer. The possible metallization of the silicon surface is also discussed. An adsorption model with secondary sites on the rest-atom dangling bonds is proposed and found to explain most of the experimental findings.

II. EXPERIMENTAL DETAILS

The Cs/Si(111)7×7 experiment was performed at the MAXLAB synchrotron-radiation laboratory at the University of Lund, Sweden. Single-crystalline silicon wafers (n^+-type doped, $\rho = 4\times10^{-3}$ Ω cm) were cleaned by resistive heating at ≈1100 °C followed by annealing to obtain high-quality Si(111)7×7 surfaces. The quality was inferred from low-energy electron diffraction (LEED) but more importantly from the intensity of surface states in ARUPS. Preparations and measurements were done in the ARUPS spectrometer connected to the toroidal grating monochromator (TGM) beamline at MAXLAB. The TGM has three interchangable gratings covering the photon-energy range 15–200 eV. Electron-energy distribution curves (EDC's) were recorded with a hemispherical electron-energy analyzer with an angular resolution of ±1.5°. Cesium was evaporated from thoroughly out-

gassed chromate dispensers (SAES Getters) at a pressure less than 5×10^{-10} Torr. The coverage was monitored through the change of the low-energy electron cutoff in UPS which corresponds to a change in the work function. The base pressure in the measurement system was below 1×10^{-10} Torr.

III. RESULTS

A. Coverage versus evaporation time

In many previous studies of alkali-metal adsorption on semiconductor surfaces (see, e.g., Ref. 8) the value of the work function, as revealed by, e.g., the secondary-electron cutoff in UPS, has been used as a reference for the coverage. Figure 1 shows the change in the work function upon adsorption of Cs on Si(111)7×7, characteristic of the evaporation conditions in the present experiment. Using synchrotron radiation from the TGM beamline at MAXLAB provides the opportunity to study also some core levels of the atomic species involved. Figure 2 shows the evolution of the peak intensities of the Cs $4d_{5/2}$ (photon energy, $h\nu=108$ eV) and the Si $2p_{3/2}$ ($h\nu=130$ eV) core-level emission for successively increased Cs evaporation times. A comparison of Figs. 1 and 2 reveals that the coverage of Cs (as monitored by the intensity of Cs $4d_{5/2}$ emission) saturates shortly before the minimum in the work function. Taking the experimental uncertainties into account, however, we believe that the saturation coverage of Cs on Si(7×7) coincides with the minimum of the work function. The intensity of Si $2p_{3/2}$ decreases over the same evaporation time period to 0.6 of the initial intensity, saturating shortly after the Cs $4d_{5/2}$ intensity.

B. Surface-state bands

The clean Si(111)7×7 surface exhibits three filled surface states labeled S_1, S_2, and S_3. In normal-emission

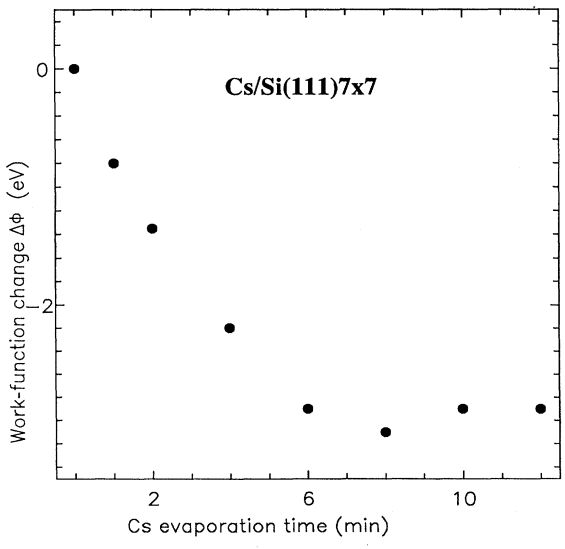

FIG. 1. The change in work function for Cs/Si(111)7×7 as a function of Cs evaporation time, derived from the change of the secondary electron cutoff in UPS.

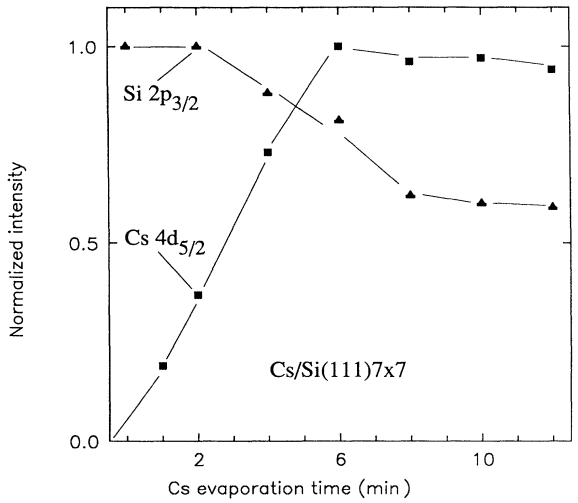

FIG. 2. Photoemission intensities of the Cs $4d_{5/2}$ and Si $2p_{3/2}$ core levels as a function of Cs evaporation time, normalized to unity at the respective maxima.

ARUPS only the two topmost states are visible: the adatom dangling-bond state S_1, which is roughly half-filled rendering the surface metallic, and the rest-atom dangling-bond state S_2. Figure 3 shows normal-emission ARUPS spectra for successive evaporations of Cs onto the Si(111)7×7 surface. For evaporation times less than 4 min the picture is quite clear. The adatom dangling-bond state S_1 (subsequently labeled $S_{1'}$) grows in intensity with evaporation time and moves away from the Fermi level. After continued evaporation the spectrum becomes almost washed out leaving a fairly smooth curve after 10

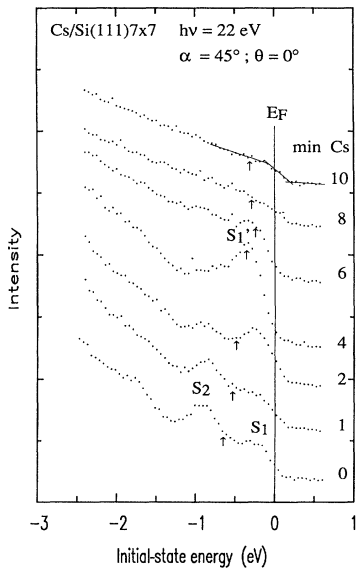

FIG. 3. Angle-resolved photoelectron spectra from the Si(111)7×7 surface for various Cs evaporation times. The photon energy was 22 eV, incidence angle 45°, and normal emission. Arrows indicate the position of the VBM as derived from Fig. 7. Straight lines have been included in the topmost spectrum to show the Fermi cutoff.

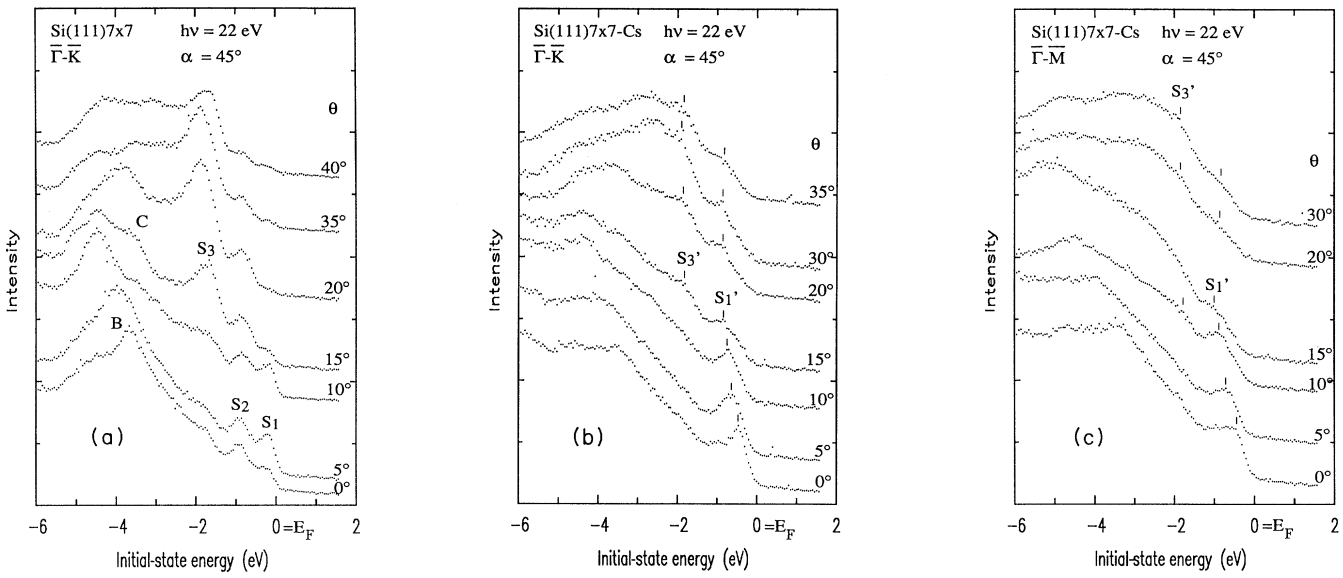

FIG. 4. Angle-resolved photoelectron spectra recorded at 45° incidence angle, photon energy 22 eV, for various angles of emission θ from (a) the clean Si(111)7×7 surface along $\bar{\Gamma}-\bar{K}$, (b) to Si(111)7×7-Cs (4 min) surface along $\bar{\Gamma}-\bar{K}$, and (c) along $\bar{\Gamma}-\bar{M}$. Energies are referenced to E_F.

min of Cs, but with increased emission at E_F where a cutoff now develops, clearly seen in the 12-min Cs spectrum. Through the entire evaporation range (< 12 min) LEED continues to show a 7×7 pattern. The position of the valence-band maximum (VBM), as derived from changes in the Si 2p binding energy with respect to E_F, is indicated with arrows in the spectra.

To gain information on the nature of the new Cs-induced surface state $S_{1'}$ and to find out to which extent it still resembles S_1 of the clean surface, we have investigated the surface band structure of the 4-min Cs surface along the two main azimuths. Figure 4 shows spectra for various angles of emission along (a) $\bar{\Gamma}-\bar{K}$ for the clean Si(111)7×7 surface, (b) $\bar{\Gamma}-\bar{K}$, and (c) $\bar{\Gamma}-\bar{M}$ for the Si(111)7×7-Cs (4 min) surface. In 4(a) the surface states S_1, S_2, and S_3 have been marked together with the bulk-band transitions, B and C, in agreement with Refs. 1–3. When approximately two-thirds of the saturation coverage of Cs has been deposited, the spectra appear as in 4(b) and 4(c). Along both directions $S_{1'}$ shows a rather strong downward dispersion in contrast to the flat S_1 band on the clean surface. Note also that a state $S_{3'}$ appears at higher angles of emission and at energies suggesting it to be related to S_3.

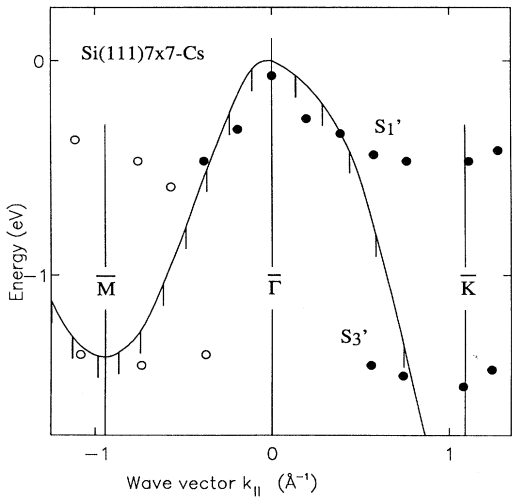

FIG. 5. The experimental surface electronic structure of Si(111)7×7-Cs. Open symbols denote weaker structures. The solid hatched line indicates the boundary of the projected valence band from Ref. 9.

The results presented in Figs. 4(b) and 4(c) have been converted into an energy versus surface wave-vector $E(k_\parallel)$ dispersion relation using the standard procedure with the proper value for the work function, $\Phi = 2.65$ eV. This is presented in Fig. 5 with the energy referenced to the VBM position at this coverage, $E_F - E_{\mathrm{VBM}} = 0.38$ eV. Included is also the hatched boundary of the projected valence band from the calculation by Ihm, Cohen, and Chelikowsky.[9] Since both $S_{1'}$ and $S_{3'}$ appear in the projected bulk band gap (e.g., at $\bar{K}$) we conclude that both structures are true surface states.

C. Core levels

The photon-energy range available at the TGM beamline allows for studies of core levels with binding energies below 200 eV, besides the demonstrated ability of ARUPS studies of valence bands and surface states. In order to study the growth of the Cs overlayer, the band bending induced and the chemical changes during growth, the emission from the 4d level of Cs and the 2p level of Si were recorded. Figure 6(a) displays the evolution of the Cs 4d photoemission intensity, $h\nu = 108$ eV,

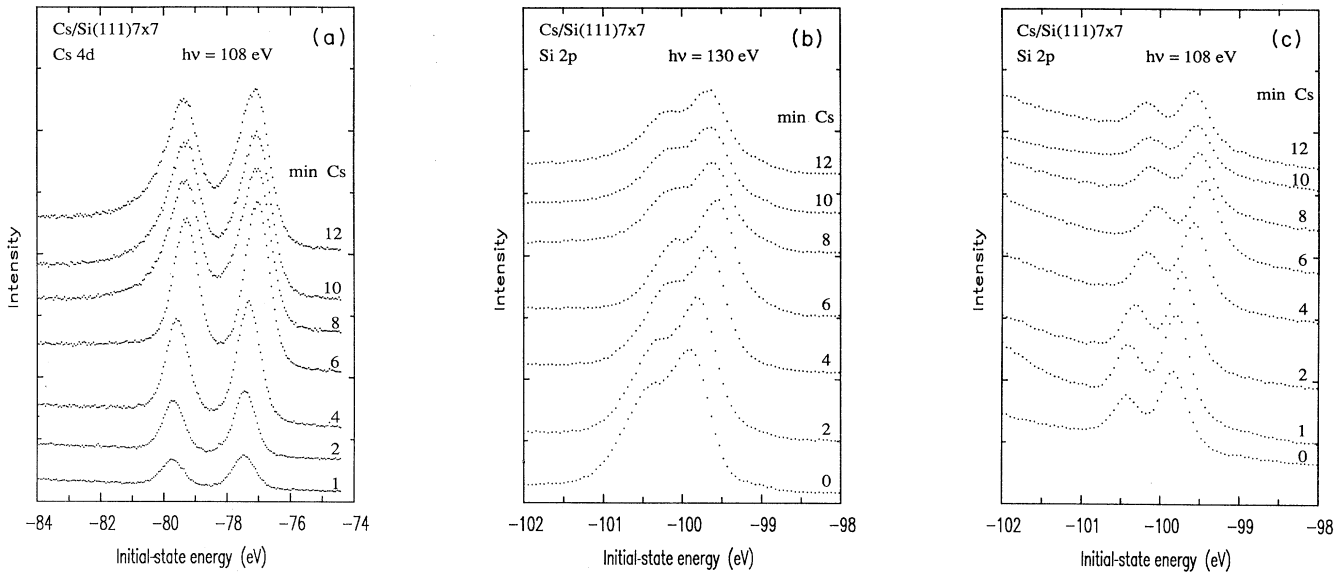

FIG. 6. Core-level photoelectron spectra recorded after various Cs evaporation times on the Si(111)7×7 surface. Panel (a) shows the development of Cs 4*d* at 108-eV photon energy while (b) and (c) show Si 2*p* recorded at photon energies 130 eV (surface-sensitive emission) and 108 eV (bulk-sensitive emission), respectively. Energies are referenced to E_F.

for successive evaporations of Cs onto the Si(111)7×7 surface. Figures 6(b) and 6(c) show the simultaneous evolution of the Si 2*p* emission, 6(b) recorded at $h\nu = 130$ eV, i.e., with high surface sensitivity, while 6(c) was recorded at $h\nu = 108$ eV, thus emphazising the emission from atoms in the bulk. The spectra have been normalized to the photon flux in order to reveal the real changes in the emission intensity. The growth of the Cs 4*d* intensity and the simultaneous decrease of the Si 2*p* intensity as displayed in Fig. 2 are clearly observed. The apparent changes in binding energies of these levels are due to our presentation of the spectra referencing the energy to the Fermi level. The adsorption of Cs changes the Fermi-energy position within the band gap of Si, i.e., induces an additional band bending. This is presented in more detail in Fig. 7, where this additional band bending due to the adsorption of Cs on Si(111)7×7, as derived from the binding-energy shifts of the bulk-sensitive Si 2*p* emission in Fig. 6(c), has been plotted versus the Cs evaporation time. These results were also the basis for the marked position of the VBM in Fig. 3. The band bending increases with Cs evaporation time and reaches a maximum of 0.38 eV after 6 min, corresponding to the completion of the saturation coverage (cf. Fig 2). With increased evaporation we note a reduction of the band bending again.

It is further interesting to study the line shapes of the core-level emissions. This can reveal chemical changes in, e.g., the bonding of Cs to Si. As can already be noted in Fig. 6(a) and is presented in more detail in Fig. 8, the line shape of the Cs 4*d* emission changes significantly between the 6-min Cs and the 8-min Cs spectra. The peak height has not changed but a strong asymmetric broadening on the high-binding-energy side has appeared. This type of broadening is well known from photoemission studies of metals and is due to final-state effects with multielectron excitations involving empty states just above E_F and filled states just below E_F,[10] i.e., it requires a local density of states on both sides of E_F. This observation shows that the Cs atoms experience a metallic local environment when the saturation coverage is completed, pointing to a metallization of the Cs overlayer.

The line shape of the Si 2*p* emission is more complex and requires a numerical deconvolution. We have used a combination of Gaussian- and Lorentzian-broadened 2*p* doublets. The results of such deconvolutions of the clean and the 12-min Cs spectra in Fig. 6(b) are presented in

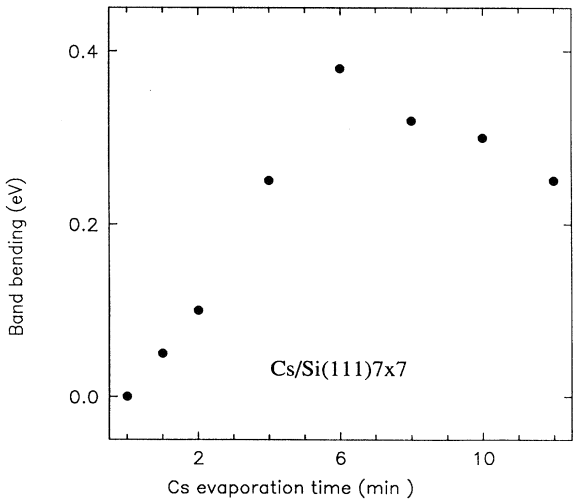

FIG. 7. The additional band bending induced by various Cs evaporation times on the Si(111)7×7 surface, derived from the shift of the Si 2*p* bulk-sensitive emission [Fig. 6(c)], with respect to E_F.

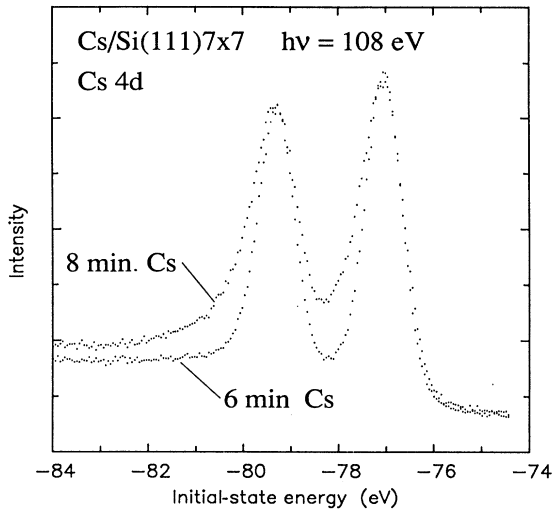

FIG. 8. Core-level photoelectron spectra from the Cs 4*d* level of the Cs/Si(111)7×7 system showing the development of an asymmetric line shape in the 8 min of Cs spectrum. The energies are referenced to E_F.

TABLE I. Numerical parameters for the fit of the Si 2*p* emission as shown in Fig. 9. Energies are given in eV; binding energies are given with respect to E_F. The Gaussian and Lorentzian full widths at half maximum were 0.40 and 0.15 eV, respectively. Both spectra were fitted with integrating backgrounds.

Si 2*p*	Si(111)7×7 clean, n^+	Si(111)7×7 12 min Cs
Spin-orbit splitting	0.614	0.614
Branching ratio	0.55	0.55
Bulk-component binding energy	99.85	99.62
Bulk-component relative intensity	0.69	0.70
Surface core-level shift $\Sigma_1, \Sigma_{1'}$	−0.32	−0.26
Relative intensity $\Sigma_1, \Sigma_{1'}$	0.28	0.20
Surface core-level shift $\Sigma_2, \Sigma_{2'}$	0.71	0.57
Relative intensity $\Sigma_2, \Sigma_{2'}$	0.03	0.10

Fig. 9. Fit parameters and results are given in Table I. The clean spectrum has been fitted with a bulk component (*B*) and two surface-shifted components (Σ_1 and Σ_2), in analogy with previous work.[11] The surface components can be interpreted as one corresponding to the adatoms and the atoms bonding to these (Σ_1) and one corresponding to the rest atoms (Σ_2) of the DAS model.[11] The values for the surface shifts from the present study, as presented in Table I, are in reasonable agreement with previous results.[11] The 12-min Cs spectrum has been fitted in a similar fashion, i.e., using one bulk (*B*) and two surface-shifted (Σ_1' and Σ_2') components. The major differences compared to the clean spectrum are changes in surface shifts and relative intensities, and an asymmetric broadening of the surface components. Firstly, both surface shifts are reduced, Σ_1 with (+)0.06 eV and Σ_2 with (−)0.14 eV. Secondly, the relative intensities change from 0.28 to 0.20 for Σ_1 and from 0.03 to 0.10 for Σ_2. Note, however, that the total surface-to-bulk intensity ratio stays constant. The third major difference is the introduction of an asymmetric broadening in the surface components. This was essential in order to achieve such a high-quality fit as displayed in Fig. 9 using only three components. The broadening is of the same kind as discussed above for the Cs 4*d* level, i.e., a Doniach-Šunjić line shape, characteristic of a material with density of states on both sides of the Fermi energy. The broadening appears already after 8 min of Cs, as evident from Fig. 6(b) where the line shape changes between the 6- and 8-min Cs spectra to remain practically unchanged upon further evaporation.

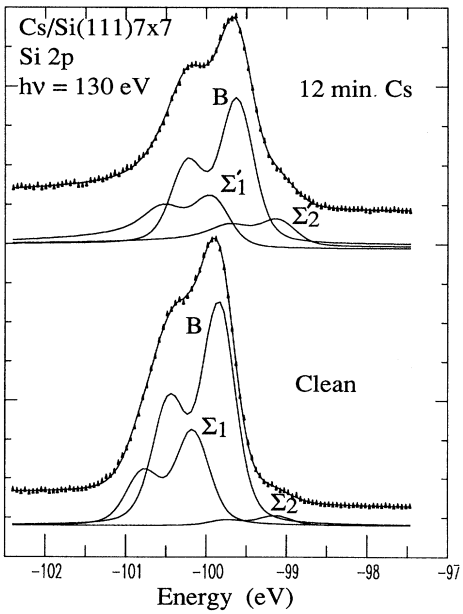

FIG. 9. The results of a numerical fitting of the Si 2*p* spectra for the clean and the 12 min of Cs surface of Cs/Si(111)7×7 from Fig. 6(b). For details see Table I.

The change in the intensities of the two surface-shifted components can be explained by calculating the observed change in surface-component intensity ratios and comparing this with a theoretical model where the intensity ratio is determined by the number of surface atoms involved and taking the attenuation into account. This is in analogy with Ref. 11. The observed intensity ratio[12] of Σ_1 changes upon adsorption of Cs from 0.39 to 0.25, i.e., by 36%. The calculated value changes by 35% if, instead of the 48 atoms on the clean surface, only 36 atoms per unit cell contribute to the emission. Remembering that the analysis of the emission from the clean surface[11] concluded that the 12 adatoms and the 36 atoms which bond to the adatoms contributed to Σ_1, we suggest that the Cs-induced core-level shift for the 12 adatoms moves the corresponding intensity from Σ_1 to $\Sigma_{2'}$ (from −0.32 eV to +0.57 eV). The increased intensity of $\Sigma_{2'}$, as compared with Σ_2, supports this proposition.

IV. DISCUSSION AND CONCLUSIONS

LEED studies show that Cs adsorbs on Si(111)7×7 conserving the 7×7 long-range order. The bonding of Cs to Si primarily takes place at the adatoms. This is evident from ARUPS through the changed electronic band structure of the adatom dangling-bond-derived surface state S_1 and from the changed surface shift of the Si 2*p* component which is due to these atoms. The Fermi level is on the clean surface pinned at 0.63 eV above the VBM (Ref. 13) by S_1, which is roughly half-filled. Upon Cs adsorption S_1 gets increasingly filled and moves down in energy with respect to E_F. At the same time Si 2*p* reveals an upward band bending, which after 4 min of Cs reaches 0.25 eV. $S_{1'}$ is at this coverage located at the VBM through the combined action of (i) $S_{1'}$ moving down from E_F due to charge donation and (ii) E_F moving down in the band gap (upward band bending) due to metal adsorption. This indicates that $S_{1'}$ is still pinning the Fermi level, but now only with the upper tail at $\bar{\Gamma}$ since the band is dispersing down away from $\bar{\Gamma}$ and is almost filled. Note further that the position of $S_{3'}$ with respect to E_F is practically unchanged compared to S_3 on the clean surface. This can only be explained by an upward shift together with the VBM due to the band bending and an almost equal shift down due to the influence from charge donation to $S_{1'}$. The changed $S_{3'}$ position with respect to the VBM of −0.2 eV is in support of this proposition.

Adsorption of Cs at every Si adatom would give an average Cs-Cs distance of 7.2 Å which is 38% larger than the nearest-neighbor distance in Cs metal (5.24 Å), the latter being close to the Mott limit for the metal-insulator transition.[14] No evidence for a second adsorption site appears in the Cs 4*d* spectra, i.e., no second 4*d* doublet appears, but we suggest that the strong surface state $S_{1'}$ (after 4 min of Cs) corresponds to the most well-ordered surface with essentially all adatom sites occupied. Further adsorption adds roughly 50% Cs atoms to reach saturation, as is evident from the Cs 4*d* intensity change in Fig. 2. We suggest this additional adsorption to take place at secondary sites, namely the rest-atom sites, bonding to these dangling bonds. Since the in-plane distance between adatoms and rest atoms is only 4.43 Å, strain is introduced within the Cs layer, forcing the atoms to separate (or buckle) to a distance larger than the distance in Cs metal. This distortion disturbs the long-range order and removes the strong surface state $S_{1'}$. The suggested second adsorption site is further supported by (1) simple atom counting—there are 12 adatoms and 6 rest atoms within the 7×7 unit cell—thus addition of 50% Cs is expected, and (2) by the fact that the surface-shifted Si 2*p* core level for the adatoms changes its energy to that of the rest atoms, as discussed above.

Adsorption in the described geometry can also explain the appearance of metallicity within the Cs overlayer by simply assuming a model where the Cs-Cs distance is locally reduced below the value for the Mott transition. Such a model would result in triangular, two-dimensional metallic clusters of 18 Cs atoms arranged within the triangles of each half unit cell of the Si(111)7×7 surface. Figure 10 shows a schematic picture of the primary adsorption at adatom sites in the left half of the unit cell and of the saturation coverage with adsorption also at rest-atom sites in the right half. The Cs atoms have been indicated with extreme radii, ionic in the left half and metallic in the right half. From the latter geometry it is clear that metallic Cs is too large and some rearrangement would in this case be necessary. Details of this model in terms of bond distances and angles require theoretical work and experiments in, e.g., x-ray diffraction and scanning-tunneling microscopy.

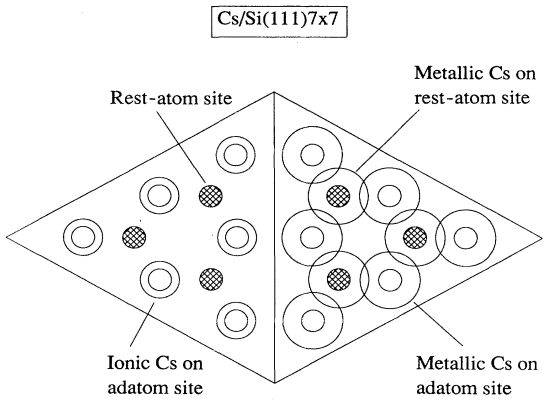

FIG. 10. Schematic illustration of the proposed adsorption model. Outlined is the 7×7 unit cell with adatom and rest-atom sites. The left half shows the adsorption of fully ionized Cs atoms at the adatom sites, while the right half indicates the case of adsorption of fully metallic Cs at adatom and rest-atom sites.

The above described model may also be used to cast some light on the appearance of dispersion for the adatom-derived $S_{1'}$ surface state. On the clean Si(111)7×7 surface S_1 is quite flat, which can be explained by the large distance between the adatom dangling bonds. What can now increase the interaction between equivalent bonds when Cs adsorbs on the surface? It is known[15] that electronic charge has been transferred from the adatom dangling bonds to the rest-atom dangling bonds on the clean surface. This difference in occupancy is (partly) responsible for the difference in energy of these two flat bands (the rest-atom dangling bonds are as far apart as the adatoms). With the Cs valence electron now filling up this charge deficiency, the energy difference between the adatom and rest-atom dangling bonds is reduced. This is explicitly observed in Fig. 3 where the energy of S_1 is lowered towards that of S_2 with increased Cs coverage. The reduced energy difference between these neighboring dangling bonds increases the mutual interaction and makes the rest-atom dangling bonds into a link between the adatom dangling bonds. Increased interaction yields increased surface band dispersion, and it is interesting to note that the energy value for $S_{1'}$ at $\bar{K}$ is close to that for S_2 on the clean surface. As a consequence of the above proposed adsorption description, the difference in energy between the adsorption sites on adatoms and on rest atoms will also become reduced. This implies that the most likely secondary adsorption sites are the rest-atom sites, in agreement with

what was proposed in the preceding part of this section, based on our observations at higher coverages.

Adsorption of Cs on Si(111)7×7, as discussed at length above, is seen to affect primarily the adatom dangling bonds in the low-coverage regime and the rest-atom dangling bonds in the higher-coverage regime, leaving the states which contribute to S_3 on the clean surface, i.e., the adatom backbonds, only indirectly affected. This then explains the appearance of $S_{3'}$ on the Si(111)7×7-Cs surface as a state which shows large similarities to S_3 on the clean surface, except for a reduction in intensity and a −0.2-eV energy shift with respect to the VBM.

V. SUMMARY

A conclusive picture for the adsorption of Cs emerges from extensive studies of the development of the Si(111)7×7-Cs surface using LEED, $\Delta\Phi$, ARUPS, and core-level photoemission. Cs is primarily bound to the Si adatom dangling bonds, producing a well-ordered surface with a strong surface state, and secondarily bound to the rest-atom dangling bonds. The saturation coverage is thus 18 Cs atoms per 7×7 surface unit cell. The surface is semiconducting with only adatom sites occupied but gets increasingly metallic as saturation is approached through adsorption also at rest-atom sites. Core-level intensities show that the saturation and work-function minimum coincide and core-level energy shifts reveal a Cs-induced maximum band bending of 0.38 eV. Dispersion of the adatom-to-Cs bond-derived $S_{1'}$ surface-state band is downward away from $\bar{\Gamma}$ through the interaction with the rest-atom dangling bonds. Core-level line shapes and the development of a Fermi cutoff show the metallization of the surface at higher coverages. Asymmetric line shapes are observed for both Cs 4*d* and the surface components of Si 2*p*, thus indicating local metallic character for both Cs and Si. Two surface-shifted Si 2*p* core levels are observed, one associated with the adatom backbonds, shifted −0.26 eV, and one associated with the adatoms and rest atoms, shifted 0.57 eV.

---

*Present address: ABB HV Switchgear AB, S-771 80 Ludvika, Sweden.

†Permanent address: Fraunhofer Institut für Mikrostrukturtechnik, Margret-Steiff-Weg 3, D-2210 Itzehoe, Federal Republic of Germany.

‡Permanent address: IBM Research Division, Zurich Research Laboratory, CH-8803 Rüschlikon, Switzerland.

[1]D. E. Eastman, F. J. Himpsel, J. A. Knapp, and K. C. Pandey, in *Physics of Semiconductors,* edited by B. L. H. Wilson (IOP, Bristol, 1978), p. 1059.

[2]F. J. Himpsel, D. E. Eastman, P. Heimann, B. Reihl, C. W. White, and D. M. Zehner, Phys. Rev. B. **24**, 1120 (1981).

[3]P. Mårtensson, W. -X. Ni, G. V. Hansson, J. M. Nicholls, and B. Reihl, Phys. Rev. B **36**, 5974 (1987).

[4]F. J. Himpsel and Th. Fauster, J. Vac. Sci. Technol. A **2**, 815 (1984).

[5]J. M. Nicholls and B. Reihl, Phys. Rev. B **36**, 8071 (1987).

[6]R. J. Hamers, R. M. Tromp, and J. E. Demuth, Phys. Rev. Lett. **56**, 1972 (1986).

[7]K. Takanayagi, Y. Tanishiro, M. Takahashi, and S. Takahashi, J. Vac. Sci. Technol. A **3**, 1502 (1985).

[8]K. O. Magnusson and B. Reihl, Phys. Rev. B **41**, 12 071 (1990).

[9]J. Ihm, M. L. Cohen, and J. R. Chelikowsky, Phys. Rev. B **22**, 4610 (1980).

[10]See, e.g., S. Hüfner and G. K. Wertheim, Phys. Rev. Lett. **35**, 53 (1975).

[11]C. J. Karlsson, E. Landemark, L. S. O. Johansson, U. O. Karlsson, and R. I. G. Uhrberg, Phys. Rev. B **41**, 1521 (1990).

[12]The intensity ratio for a surface component is defined as the ratio between the area of this component and the sum of the areas of the bulk and the second surface component.

[13]F. J. Himpsel, G. Hollinger, and R. A. Pollak, Phys. Rev. B **28**, 7014 (1983).

[14]A. Ferrez, N. H. March, and F. Flores, J. Phys. Chem. Solids **45**, 627 (1983).

[15]J. E. Northrup, Phys. Rev. Lett. **57**, 154 (1986).